Author/s:
Yu, H;Palazzolo, JS;Zhou, J;Hu, Y;Niego, B;Pan, S;Ju, Y;Wang, T-Y;Lin, Z;Hagemeyer, CE;Caruso, F

Title:
Bioresponsive Polyphenol-Based Nanoparticles as Thrombolytic Drug Carriers

Date:
2022-01-12

Citation:
Yu, H., Palazzolo, J. S., Zhou, J., Hu, Y., Niego, B., Pan, S., Ju, Y., Wang, T. -Y., Lin, Z., Hagemeyer, C. E. & Caruso, F. (2022). Bioresponsive Polyphenol-Based Nanoparticles as Thrombolytic Drug Carriers. ACS APPLIED MATERIALS & INTERFACES, 14 (3), https://doi.org/10.1021/acsami.1c19820.

Persistent Link:
https://hdl.handle.net/11343/297204

Bioresponsive Polyphenol-Based Nanoparticles as Thrombolytic Drug Carriers

Haitao Yu,[a,‡] Jason S. Palazzolo,[b,‡] Jiajing Zhou,[a,‡] Yingjie Hu,[a] Be'eri Niego,[b] Shuaijun Pan,[a] Yi Ju,[a] Ting-Yi Wang,[b] Zhixing Lin,[a] Christoph E. Hagemeyer,[b,] and Frank Caruso[a,*]*

[a]Department of Chemical Engineering, The University of Melbourne, Parkville, Victoria 3010, Australia

[b]NanoBiotechnology Laboratory, Australian Centre for Blood Diseases, Central Clinical School, Monash University, Melbourne, Victoria 3004, Australia

*Corresponding authors. E-mail: fcaruso@unimelb.edu.au (F. C.); christoph.hagemeyer@monash.edu (C. E. H.)

[‡]H.Y., J.S.P., and J.Z. contributed equally to this work

KEYWORDS thrombolytic nanoparticles, polyphenol, plasminogen activators, urokinase, thrombin-cleavable peptide

ABSTRACT

Thrombolytic (clot-busting) therapies with plasminogen activators (PAs) are first-line treatments against acute thrombosis and ischaemic stroke. However, limitations such as narrow therapeutic

windows, low success rates, and bleeding complications hinder their clinical use. Drug-loaded polyphenol-based nanoparticles could address these shortfalls by delivering a more targeted and safer thrombolysis, coupled with advantages such as improved biocompatibility and higher stability in vivo. Herein, a template-mediated polyphenol-based supramolecular assembly strategy is used to prepare nanocarriers of thrombolytic drugs. A thrombin-dependent drug release mechanism is integrated using tannic acid (TA) to cross-link urokinase-type PA (uPA) and a thrombin-cleavable peptide on a sacrificial mesoporous silica template via noncovalent interactions. Following drug loading and template removal, the resulting nanoparticles retain active uPA and demonstrate enhanced plasminogen activation in the presence of thrombin (1.14-fold; $p < 0.05$). Additionally, they display lower association with macrophage (Raw 264.7) and monocytic (THP-1) cell lines (43% and 7% reduction, respectively), reduced hepatic accumulation and delayed blood clearance in vivo (90% clearance at 60 min vs. 5 min) compared with the template-containing nanoparticles. Our thrombin-responsive, polyphenol-based nanoparticles represent a promising platform for advanced drug delivery applications, with potential to improve thrombolytic therapies.

1. INTRODUCTION

Acute thrombosis, a pathological hemostatic condition, is a leading cause of morbidity and mortality worldwide.[1–3] Thrombosis occurs when blood clots (known as thrombi) form within blood vessels. These blood clots can result in vascular occlusions that disrupt blood supply to vital organs downstream, leading to severe organ damage.[4] In the fields of biomedicine and biotechnology, protein-based therapeutics have received much interest owing to their relatively high specificity and low side effects.[5–9] Specifically, in the context of thrombolysis, first-line treatments using plasminogen activators (PAs) have been used as leading approaches for thrombus

dissolution.[10–12] However, the systemic delivery of PAs is clinically limited by several factors, including their rapid neutralization by endogenous inhibitors (e.g., plasminogen activator inhibitor-1)[13,14] and high risk of severe side effects (e.g., haemorrhagic complications),[15] resulting in decreased therapeutic outcomes and compromised risk–benefit profiles. Among the PAs of interest, urokinase plasminogen activator (uPA) is inexpensive and widely used for the treatment of acute ischaemic stroke in developing countries. Although effective, its use is associated with a high risk of intracranial bleeding as it lacks fibrin specificity.[12,16] A pressing need therefore exists to develop improved PA delivery systems (particularly for uPA in stroke) to achieve more effective and safe thrombolysis outcomes.

Thrombolytic drugs are designed to enrich and selectively act at sites of pathological thrombosis while sparing healthy haemostatic processes. Accordingly, much effort has been devoted to realizing the site-specific delivery of PAs by exploiting the biological microenvironment of thrombi, including high shear stress levels,[17,18] associated coagulation factors, like thrombin,[19,20] and active targeting against thrombi-specific markers.[21,22] Emerging nanotechnologies demonstrate their potential for achieving enhanced thrombolytic treatment outcomes while offering improved safety profiles;[23] these include the development of magnetic nanoparticles (NPs),[24] electrostatically charged NPs,[25] as well as lipid-based NPs.[26] These NPs are aimed at improving PA loading capacities while serving as a thrombin-responsive drug delivery platform to transport PAs locally to thrombi. However, various NP systems still face limitations that may hinder future clinical translation. For example, magnetic NPs can exhibit poor biocompatibility and their application requires sophisticated infrastructure for their therapeutic application,[24] such as a rotating magnetic field, which may limit patient accessibility. Therefore, the development of

NP platforms that enable both thrombus site-specific delivery and effective in vivo performance is of interest.

Polyphenol-based assemblies have received significant interest because of their potential in biomedical and other applications, owing to their broad adherence to diverse substances, noncovalent interactions, and responsive properties.[9,27–33] Tannic acid (TA), a naturally occurring polyphenol, can interact with, for example, various metal ions and diverse macromolecules, via hydrophobic interactions, covalent bonding, hydrogen bonding, electrostatic interactions, metal coordination, and π interactions. In the present study, a TA-based strategy was used to synthesize bioresponsive NPs of controllable sizes, consisting of an encapsulated protein drug and an activation-triggering peptide. Specifically, sacrificial mesoporous silica (MS) NP templates were loaded with the thrombolytic drug uPA. The uPA-loaded MS NP templates were subsequently incubated with TA and a thrombin-cleavable low-fouling peptide (Pep) to generate MS@uPA/Pep/TA NPs. Following template removal, uPA/Pep/TA NPs were obtained, displaying reduced nonspecific cell association, delayed blood clearance, good preservation, and control of uPA activity, and a thrombin-responsive uPA release capacity compared with the template NPs (i.e., control). These findings are fundamental for future engineering of functional polyphenol-based NPs for advanced biomedical applications.

2. EXPERIMENTAL SECTION

2.1. Materials. TA (ACS reagent), urea, Tween 20, NaCl, phenazine methosulfate (PMS), dimethyl sulfoxide (DMSO), bovine serum albumin (BSA), and human plasminogen were purchased from Sigma-Aldrich (St. Louis, MI, USA). Urokinase for injection (U-FRAG, lyophilized) was purchased from medac GmbH (Wedel, Schleswig-Holstein, Germany). Thrombin enzyme was obtained from Global Siemens Healthcare (Erlangen, Bavaria, Germany). Carboxylic

acid-functionalized polystyrene particles (1.86 ± 0.03 μm) were purchased from microParticles GmbH (Berlin, Germany). Dulbecco's phosphate buffered saline (DPBS), Dulbecco's modified Eagle medium (DMEM), Alexa Fluor 647 succinimidyl ester (AF647 NHS ester), Alexa Fluor 488 succinimidyl ester (AF488 NHS ester), and 2,3-bis[2-methoxy-4-nitro-5-sulfophenyl]-2*H*-tetrazolium-5-carboxanilide inner salt (XTT) were purchased from Life Technologies (Melbourne, Victoria, Australia). Cyanine7.5 NHS ester (Cy7.5 NHS) was purchased from Lumiprobe (Hunt Valley, MD, USA). A low-fouling, custom-made peptide H_2N-GGGPAAPAPS APAASPAAPS ELTPRGWRLE SAPAASPAAP APASPAAPAA ELTPRGWRLE AASPAAPAPS APAPASPAAA-COOH, containing proline–alanine–serine (PAS) in the backbone, was obtained from Shanghai Apeptide Co., Ltd. (Shanghai, China). Figure 1a shows a schematic representation of the structure of the peptide: its molecular weight is ~6.9 kDa, and each peptide integrates two 10-mer peptide sequences with two thrombin-cleavable sites (ELTPRGWRLE). High-purity Milli-Q water with a resistivity of 18.2 MΩ cm was obtained from an inline Millipore RiOs/Origin water purification system and was used in all experiments. All chemicals were used without any further purification. S-2251 chromogenic substrate was purchased from Chromogenix (Bedford, MA, USA). Human thrombin (high activity) was purchased from EMD Millipore (Burlington, MA, USA). Ketamine hydrochloride (Ketamav 100) was purchased from Mavlab (Logan City DC, Queensland, Australia). Xylazine hydrochloride (ilium Xylazil-20) was obtained from Troy Animal Healthcare (Glendenning, New South Wales, Australia).

2.2. Assembly of uPA/Pep/TA NPs. The uPA/Pep/TA NPs were prepared via a MS template-assisted assembly technique, which allowed control of the size and structure of the NPs, as shown in our previous studies on polymer NPs.[34,35] First, MS NP templates with large, interconnected pores were synthesized according to the anion-assisted protocol detailed therein.[36] Monodisperse

MS NPs were obtained via sonication in a sonication bath for 10 min. Then, an MS NP dispersion (50 µL, 10 mg mL^{-1} in water) and uPA (100 µL, activity concentration of 1.57 mg mL^{-1} (250,000 U mL^{-1}) in excess amount were added to water (350 µL) and incubated overnight on a rotary wheel. A final MS NP concentration of 1 mg mL^{-1} was used as the optimized condition to load uPA (higher MS NP concentrations resulted in particle aggregation).

The uPA-loaded MS NPs (MS@uPA NPs) were subsequently centrifuged at 5000 *g* for 5 min. The supernatant was discarded and the MS@uPA NPs were resuspended in water (500 µL) using a sonication bath. The centrifugation–redispersion procedure was repeated two more times to ensure removal of free uPA, subsequently generating an MS@uPA NP stock dispersion. To introduce the peptide, a polyphenol-based process was adopted as follows. The MS@uPA NP stock dispersion (50 µL) was first diluted in water (450 µL). The peptide in DPBS solution (40 µL, 2 mg mL^{-1}) was then added to the MS@uPA NP dispersion and mixed by vortexing for 10 s. A TA aqueous solution (40 µL, 0.5 mg mL^{-1}, pH = 4.3) was subsequently added and mixed by vortexing (10s). The resulting dispersion was incubated for 1 h, after which the particles were spun down by centrifuging at 5000 *g* for 5 min and then resuspended in water to remove excess peptide and TA. This polyphenol-based process was repeated three times to produce MS@uPA/Pep/TA NPs. The MS NP template was removed with 2 M HF/3 M NH_4F buffer solution. *Caution! HF is highly toxic and only small quantities should be prepared and handled with extreme care.* The final uPA/Pep/TA NPs were washed three times with water (centrifuging at 8000 *g* for 5 min and then redispersing using a sonication bath) to remove residual HF.

To identify the predominant interactions operating within the assembled uPA/Pep/TA NPs, a dispersion (20 µL) of the as-prepared uPA/Pep/TA NPs was diluted in water (70 µL) and then mixed with a solution (10 µL) of urea (100 mM), Tween 20 (100 mM), or NaCl (100 mM).

Changes in the NP size were monitored over 24 h via dynamic light scattering (DLS) measurements.

We examined the stability of the protein/Pep/TA NPs in human plasma by monitoring any changes in particle size using DLS. The BSA/Pep/TA NPs were incubated in human plasma for 0 and 24 h at 37 °C, respectively, and then washed/redispersed with water (i.e., centrifuged at 8000 *g* for 5 min, the supernatant exchanged, and redispersed using a sonication bath) at least three times before DLS measurements.

2.3. Plasminogen Activation of uPA after HF Treatment. A carboxylic acid-functionalized polystyrene particle dispersion (25 µL, 1.86 ± 0.03 µm, 100 mg mL^{-1} in water) and uPA (50 µL, activity concentration of 1.57 mg mL^{-1} (250,000 U mL^{-1})) were added to water (425 µL) and incubated overnight on a rotary wheel. Then, the uPA-loaded polystyrene particles were centrifuged at 3000 *g* for 2 min. The supernatant was discarded and the uPA-loaded polystyrene particles were resuspended in water (500 µL) using a sonication bath. The centrifugation–redispersion procedure was repeated two more times to ensure removal of free uPA in bulk.

Subsequently, the uPA-loaded polystyrene particle dispersion (200 µL) was added to 2 M HF/3 M NH_4F buffer solution (200 µL) or DPBS buffer solution (200 µL, as control), mixed by vortexing for 10 s, and incubated for 10 min. Finally, both the uPA-loaded polystyrene particle dispersions after HF treatment and DPBS buffer solution were washed at least three times with water (centrifuging at 3000 *g* for 2 min and then redispersing by vortexing) to remove residual HF.

The plasminogen activation of both the uPA-loaded polystyrene particle dispersions following HF treatment and DPBS treatment was measured at a concentration of 1.7×10^6 particles mL^{-1} according to the procedure described in Section 2.5.

2.4. Fluorescence Pre-Labeling of Protein and Peptide. Fluorescence pre-labeling of uPA, BSA, and the peptide was achieved via *N*-hydroxysuccinimide (NHS) chemistry between the amine residues in the protein or peptide and AF647 NHS or AF488 NHS, respectively. Briefly, uPA (680 µL, 1.57 mg mL^{-1}) or BSA (500 µL, 2 mg mL^{-1}) in phosphate-buffered saline (PBS) buffer was mixed with AF647 NHS (20 µL, 1 mg mL^{-1} in DMSO), whereas the peptide (480 µL, 2 mg mL^{-1} in PBS buffer) was mixed with AF488 NHS (20 µL, 1 mg mL^{-1} in DMSO). The NHS reaction was allowed to proceed for 3 h with gentle incubation before a desalting spin column step (dextran 7 kDa cutoff, Pierce/Thermo Scientific, IL, USA) was undertaken to remove excess unreacted dyes. Standard curves of AF647-uPA (excitation 633 nm, emission 665 nm) and AF488-peptide (excitation 490 nm, emission 525 nm) in aqueous solutions were measured using an Infinite M200 PRO multimode microplate reader (Tecan), see Figure S2. The fitting equations are $I_{665\ nm} = 51.26C_{uPA}$ and $I_{525\ nm} = 51.26C_{Pep}$, where $I_{665\ nm}$ and $I_{525\ nm}$ are the intensities at 665 and 525 nm, respectively, and C_{uPA} and C_{Pep} represent the concentrations of uPA and peptide in solution (µg mL^{-1}), respectively. The fluorescence of uPA/Pep/TA NPs was measured on a Fluorolog spectrofluorometer (Horiba Scientific, UK) at excitation wavelengths of 475 nm and 620 nm.

For the in vivo biodistribution and blood clearance studies, BSA was fluorescently labeled by mixing Cy7.5 NHS (0.4 mg), reconstituted in 100% DMSO, with BSA (30 mg). The dye-labeling reaction was allowed to incubate at room temperature (22 ℃) for 5 h with frequent mixing. Thereafter, the mixture was spun at 4000 *g* for 10 min using Amicon Ultra-4 10 kDa molecular weight cutoff centrifugal filter devices (Merck Millipore, MA, USA). The filtrate was discarded and the captured material resuspended in PBS and spun again. The resuspension and washing steps were repeated until a transparent filtrate was obtained, which indicates the absence of unbound

Cy7.5 NHS molecules. The Cy7.5-labeled BSA product was finally resuspended in PBS (800 µL) and stored at −80 °C until use. The reaction mixture was shielded from light throughout the process.

2.5. Plasminogen Activation Assay. To measure the plasminogen activation of the uPA-loaded NPs, reaction mixtures were prepared on a transparent 96-well plate (Corning Life Sciences, NY, USA), comprising the NPs (MS@uPA NPs, MS@uPA/Pep/TA NPs, or uPA/Pep/TA NPs; 25 µL, 3.6×10^6 particles mL^{-1}), S-2251 (0.5 mM), and reaction buffer (50 mM HCl with 0.01% Tween 80, pH 7.4). To initiate the reaction, human plasminogen (25 µL, 0.5 µM) and human thrombin (0 (control), 1, or 2.5 U mL^{-1}) were added immediately before absorbance measurements were performed. The absorbance at 405 nm as a function of reaction time was measured for 240 min with intervals of 60 s (20 flashes per well, shaking before each cycle) on a FLUOstar OPTIMA microplate reader (BMG Labtech, Australia) set at 37 °C. All concentrations stated in the present work represent the final concentrations in the 125 µL reaction.

2.6. Cell Culture. Raw 264.7 cells and THP-1 cells were purchased from the American Type Culture Collection and cultured in complete DMEM containing 10% fetal bovine serum at 37 °C in a cell culture incubator with 5% CO_2 and 95% humidity.

2.7. Cell Cytotoxicity. Cells were seeded at a density of 1×10^4 cells per well in triplicate in 96-well microplates overnight. The NPs were added and incubated with the cells for 48 h. After incubation, the culture medium was replaced with fresh medium containing activated XTT (0.2 mg mL^{-1}; 10 mL of 0.2 mg mL^{-1} XTT in complete medium was activated by adding 20 µL of 1 mM PMS in DPBS), and cells were allowed to incubate further at 37 °C for 3 h. Cell viability was measured on an Infinite M200 microplate reader (Tecan, Switzerland) at 475 nm, with 675 nm as

the reference wavelength. Cell viability is expressed as a percentage by normalizing absorbance to untreated cells.[37]

2.8. Cell Association. Cells were seeded at a density of 10^5 per well in 24-well plates and incubated at 37 °C overnight. The fluorescently labeled NPs were added and incubated with cells for 1 and 12 h. Then, the cells were gently washed with DPBS to remove nonassociated NPs (the adherent cells were treated with 0.25% trypsin at 37 °C for 5 min to allow detachment) and collected via centrifugation at 350 *g* for 5 min. The resulting pellet was then resuspended in DPBS and analyzed on an Apogee A50-Micro flow cytometer. At least 10^4 cells were analyzed for each sample. Cell association of the NPs was evaluated as the percentage of cells that exhibited stronger fluorescence intensity than untreated cells.

2.9. In Vivo Biodistribution and Blood Clearance Studies. In vivo studies were conducted using C57Bl/6 male mice aged 8–12 weeks (purchased from the Alfred Research Alliance Precinct Animal Centre, Australia). All animal experiments were approved by the Alfred Research Alliance Animal Ethics Committee, Monash University (AEC number E/1625/2016/M). Prior to injection, the mice were distributed into either 1 or 24 h timepoint groups. All mice were anesthetized with ketamine (100 mg kg^{-1}) and xylazine (10 mg mL^{-1}) administered via intraperitoneal (IP) injection. When no longer responsive to toe pinch stimulation, the mice were administered Cy7.5-labeled BSA at a dose of 3 μL per gram body weight via the tail vein. Cy7.5-labeld BSA was encapsulated within either the template-containing NPs (MS@Cy7.5-BSA/Pep/TA NPs; stock concentration 4.0 × 10^{11} particles mL^{-1}) or the template-free NPs (Cy7.5-BSA/Pep/TA NPs; stock concentration 8.5 × 10^{10} particles mL^{-1}).

Blood samples were then collected by clipping the mouse tail (no more than 2 mm from the tip) and withdrawing blood (2.5 μL) using a pipette at the following timepoints post injection: 2.5, 5,

10, 30, and 60 min (from mice in the 1 h timepoint group), and 120, 240, 360 min, and 24 h (from mice in the 24 h endpoint group). The concentration at time $t = 0$ was estimated by performing a 1/20 dilution of both NP stock solutions in naïve mouse blood, assuming that each mouse has an estimated 60 mL kg^{-1} of total circulating blood (i.e. ~1.5 mL for an average 25 g mouse).[38] Therefore, when dosed at 3 µL g^{-1} (75 µL in total for a 25 g mouse), an approximate dilution factor of 20 occurs in the bloodstream. Blood samples were carefully pipetted onto microscope slides, allowed to dry while shielded from light at room temperature, and stored in the dark at 2–8 °C until imaging. Notably, the fluorescence values of the estimated $t = 0$ samples were reasonably higher than those obtained at the earliest sampling timepoint (2.5 min).

After the final blood collection, the mice were euthanized by an overdose IP injection of ketamine/xylazine (300/30 mg/kg, respectively) and subsequently subjected to transcardial perfusion with PBS (20 mL) before the liver, spleen, kidney, heart, and lung were harvested. The organs were briefly washed and stored in PBS at 2–8 °C and in the dark until fluorescence imaging was performed. The scans were recorded on an Odyssey CLx scanner (LI-COR Biosciences, NE, USA), with the fluorescence detected using the 800 nm line. The total fluorescence intensity values (FU) were extracted for each sample, as well as the total fluorescence of each injected dose, calculated from a standard curve of stock volume vs. FU. The percentage (%) of remaining material, for blood clearance, and the percentage (%) of injected dose per gram tissue, for biodistribution, were calculated according to the formulae below:

$$\text{Blood Clearance (\%)} = \frac{I_t}{I_0} \times 100 \quad (1)$$

where I_t and I_0 represent the blood fluorescence intensity at a given timepoint t and at $t = 0$, respectively.

$$\text{Biodistribution (\% injected dose/g)} = \frac{(I_0/I_d) \times 100}{w_0} \quad (2)$$

where I_0 and I_d are the total fluorescence intensity of a given organ and dose, respectively, and w_0 is the total weight of a given organ.

2.10. Statistical Analyses. For the plasminogen activation assay, statistical analyses were performed using GraphPad Prism version 7.01 (GraphPad Software, CA, USA). Absorbance values at 405 nm were first plotted against time and all absorbance values greater than 0.5 were excluded from the analysis. The remaining data were fitted with a second-order polynomial (quadratic) nonlinear regression ($Y = A + BX + CX^2$). The resulting equation was then twice differentiated to yield the rate constant of plasminogen activation ($2 \times C$). Comparisons between three groups or more were performed by one-way ANOVA with uncorrected Fisher's least significant difference post-hoc analysis. A p value of <0.05 was considered significant. For the biodistribution and blood clearance studies, statistical analysis was performed using Microsoft Office Excel and GraphPad Prism version 7.01.

2.11. Minimum Information Reporting in Bio–Nano Experimental Literature (MIRIBEL). The studies conducted herein, including material characterization, biological characterization, and experimental details, conform to the MIRIBEL reporting standard for bio–nano research,[39] and we include a companion checklist of these components in the Supporting Information.

2.12. Characterization. Transmission electron microscopy (TEM) analysis of the NPs was performed on an FEI Tecnai Spirit transmission electron microscope (FEI, OR, USA) at an operation voltage of 80 kV. The TEM samples were prepared by dropping the diluted samples (10 μL) on formvar carbon-coated copper grids and subsequently drying them overnight. Scanning electron microscopy (SEM) images were captured on an FEI Quanta 200 field-emission scanning electron microscope operating at an accelerating voltage of 10 kV. The SEM samples were dried and gold-sputtered prior to imaging. Atomic force microscopy (AFM) analysis was conducted on

a Cypher S instrument (Asylum Research, CA, US). To determine the size distribution of the NPs, DLS analysis was performed on a Zetasizer Nano ZS instrument (Malvern Instrument, Worcestershire, UK). The ζ-potentials of the NPs were determined on a Zetasizer Nano ZS instrument. Solutions of the NPs obtained at each step during the synthesis were diluted 20× in water. The refractive indices of the protein and water were 1.45 and 1.33, respectively. Fourier transform infrared (FTIR) spectroscopy analysis was carried out on a Tensor II FTIR spectrophotometer (Bruker). Confocal microscopy images were captured on a Nikon A1R+ confocal laser scanning microscope (Nikon Corporation, Japan).

3. RESULTS AND DISCUSSION

(a) Thrombin-cleavable peptide

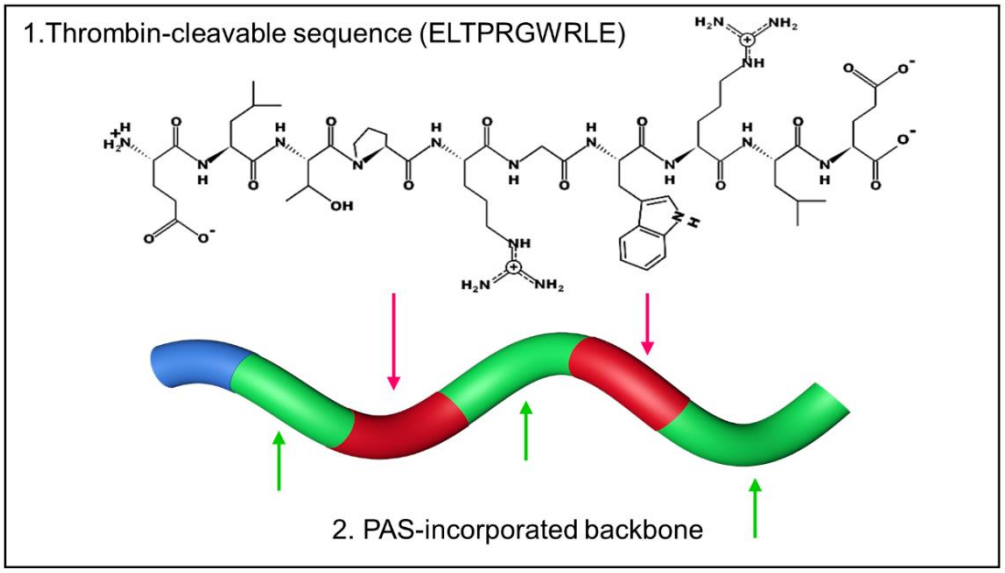

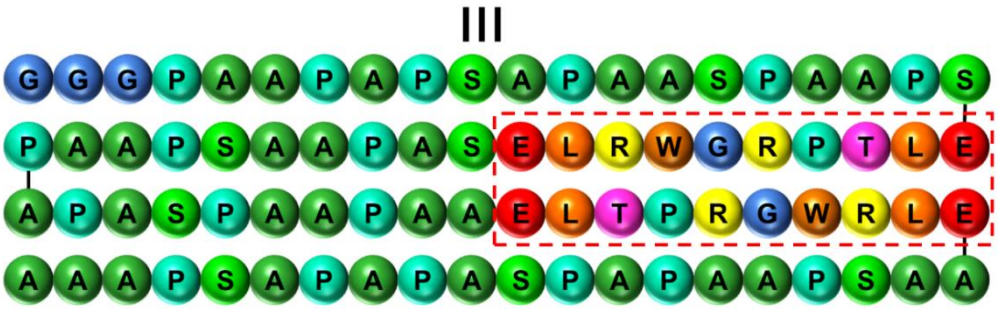

(b) Polyphenol-based strategy

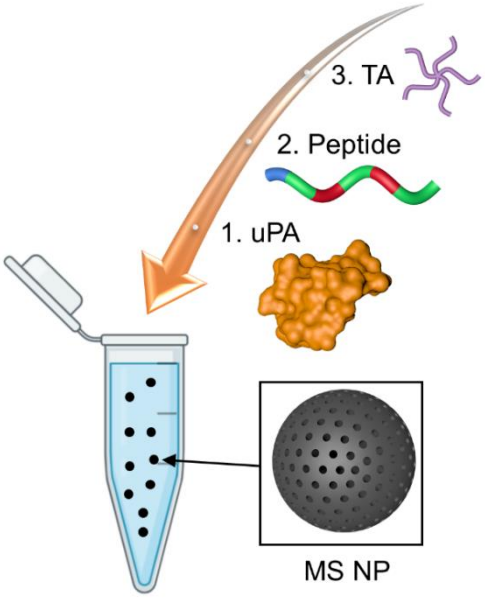

(c) MS@uPA/Pep/TA NP

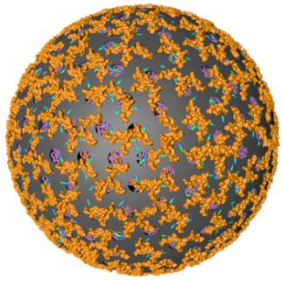

(d) uPA/Pep/TA NP

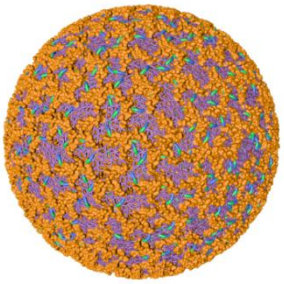

Figure 1. (a) Representation of the peptide employed herein featuring two thrombin-cleavable sequences (ELTPRGWRLE) and a PAS-incorporated backbone. Schematic diagrams of (b) the synthesis of bioresponsive polyphenol-based NPs using MS NP templates and (c, d) the multi-bioresponsive NPs before and after MS NP template removal, respectively.

3.1. Assembly of uPA/Pep/TA NPs. The MS NP templates, which were used as sacrificial nanocarrier templates, were loaded with uPA before complexation with a multifunctional peptide (Figure 1a) and TA, as shown in Figure 1b, to produce MS@uPA/Pep/TA NPs (Figure 1c). The protein–PepTA NPs (i.e., uPA/Pep/TA NPs, shown in Figure 1d) were obtained after MS NP template removal with 2 M HF/3 M NH_4F buffer solution. The size distributions (obtained by DLS) and ζ-potentials of the NPs at the different steps of the synthesis are shown in Figure 2a,b. The MS templates displayed a uniform diameter (*Z*-average) of ~270 nm, polydispersity index (PDI) of 0.057, and a specific surface area of 915 $m^2\ g^{-1}$, according to the SEM, TEM, and Brunauer–Emmett–Teller results in Figure S1. Following incubation of the MS NP templates in excess uPA for 12 h with gentle mixing (allowing adequate diffusion and interaction between the uPA and MS NPs), MS@uPA NPs displayed a small increase in size to ~290 nm and PDI of 0.082. However, MS@uPA NPs displayed a considerably less negative ζ-potential of −12 mV than MS NPs (−30 mV), indicating successful loading of the positively charged uPA. The specific loading amount of uPA in the MS@uPA NPs was calculated as 4.4 $\mu g\ mL^{-1}$ by measuring the fluorescence intensity at 665 nm of AF647-labeled uPA (Table S1 and Figure S2). Subsequent complexation between TA and MS@uPA/Pep NPs and removal of MS NP template did not induce any significant further changes in the size of the NPs. The uPA/Pep/TA NPs were monodisperse with a size of 305.2 nm and PDI of 0.128. The ζ-potential of the MS@uPA/Pep/TA NPs became more negatively charged (−25 mV) upon complexation of TA during the polyphenol-based process. The

ζ-potential of the uPA/Pep/TA NPs increased to –21 mV after the negatively charged MS NP template was removed.

The dominant interactions driving the assembly of the uPA/Pep/TA NPs were examined by incubating the particles in urea (10 mM), Tween 20 (10 mM), or NaCl (10 mM), respectively. Urea, Tween 20, and NaCl can participate in hydrogen bonding, hydrophobic interactions, and electrostatic interactions, respectively. As shown in Figure 2c, the uPA/Pep/TA NPs were stable in urea and NaCl following incubation for 24 h, whereas they rapidly disassembled once incubated in Tween 20. These findings indicate that hydrophobic interactions among the protein, peptide, and TA were the dominant interaction driving the assembly of the NPs.

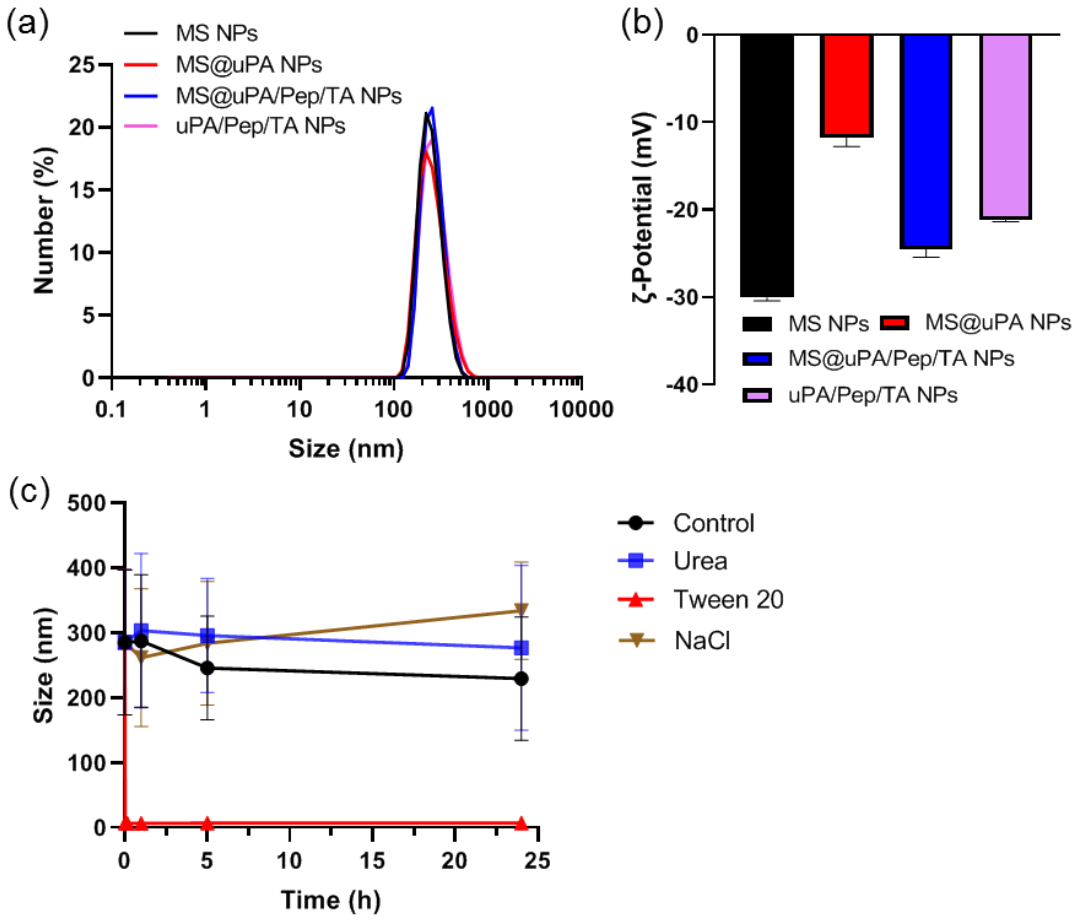

Figure 2. (a) Size distribution profiles from DLS measurements and (b) ζ-potential values of the NPs (MS NPs, MS@uPA NPs, MS@uPA/Pep/TA NPs, and uPA/Pep/TA NPs) obtained at different steps during the synthesis. (c) Average size (distribution peak average measured by DLS) of uPA/Pep/TA NPs following incubation in different solutions (PBS (control), 10 mM urea, Tween 20, or NaCl) as a function of time. The error bars represent the standard deviation (SD) of particle size.

The MS@uPA NPs, MS@uPA/Pep/TA NPs, and uPA/Pep/TA NPs were also characterized by TEM (Figure 3a–f). For sample preparation, a dispersion of the NPs was cast and allowed to dry on formvar carbon-coated copper grids, resulting in slight adhesion and aggregation of the NPs, especially for the uPA/Pep/TA NPs. The size of the NPs with MS (MS@uPA NPs and MS@uPA/Pep/TA NPs) was ~230 nm, which agrees with that measured in solution by DLS. In contrast, the uPA/Pep/TA NPs were only ~130 nm in size, which corresponds to a reduction of ~50% (vs. ~300 nm in solution, Figure 2a). The AFM results in Figure 3g,h confirmed that the height of the uPA/Pep/TA NPs on a silica wafer substrate was ~120 nm. The size shrinkage of the uPA/Pep/TA NPs indicates the porous structure and soft nature of the particles.

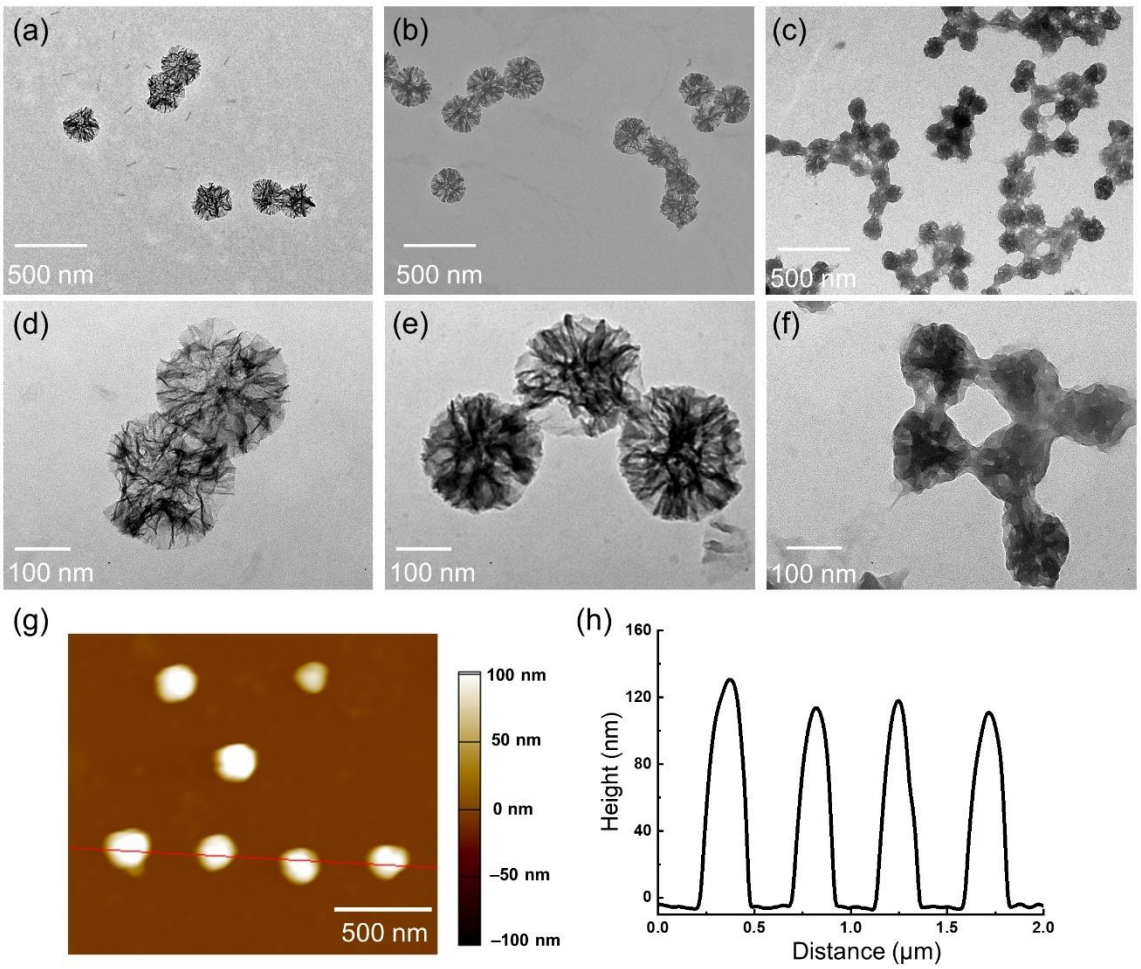

Figure 3. (a–c) Low- and (d–f) high-magnification TEM images of MS@uPA NPs (a, d), MS@uPA/Pep/TA NPs (b, e), and uPA/Pep/TA NPs (c, f). (g) AFM image and (h) corresponding cross-sectional height profiles of uPA/Pep/TA NPs.

The uPA/Pep/TA NPs were further characterized using confocal microscopy and spectrofluorometry. To visualize the NPs, uPA was labeled with AF647, whereas the peptide was labeled with AF488. In the confocal microscopy images shown in Figure 4a–c, the fluorescence of AF647-uPA and AF488-peptide in uPA/Pep/TA NPs was detected using excitation wavelengths of 633 and 488 nm and overlapped with each other, indicating the successful complexation of the protein and peptide by using TA via noncovalent interactions (dominated by hydrophobic

interactions according to Figure 2c) in the NPs. The coexistence of uPA and the peptide was also supported by the peaks observed at 515 and 675 nm in the emission curves (Figure 4d,e). The fluorescence intensities of the MS@uPA NPs and MS@uPA/Pep/TA NPs were measured using a microplate reader to identify the mass ratio of the uPA and peptide according to the standard curves of AF647-uPA and AF488-peptide in Figure S2. As listed in Table S1, the uPA/peptide mass ratio was 4.48:1, corresponding to a molar ratio of 0.71:1 considering the molecular weight of the peptide (6.9 kDa) and the molecular weight (43.5 kDa) of uPA (averaged from two forms of uPA with low (33 kDa) and high (54 kDa) molecular weight). In addition, FTIR analysis confirmed the presence of BSA, peptide, and TA in the BSA/Pep/TA NPs (Figure S3).

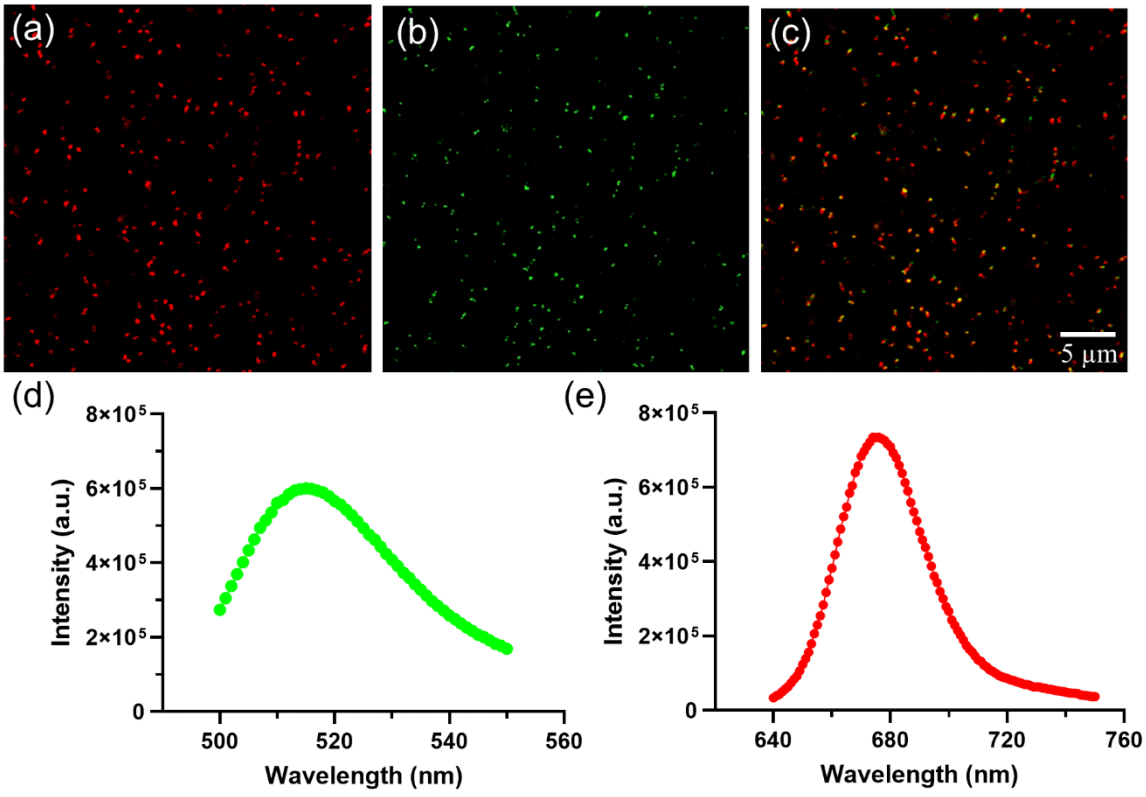

Figure 4. (a–c) Fluorescence images of uPA/Pep/TA NPs in the 633 nm channel (a), 488 nm channel (b), and overlay (c) obtained by confocal microscopy. uPA was pre-labeled with AF647

and the peptide was pre-labeled with AF488. (d, e) Emission spectra of uPA/Pep/TA NPs obtained at excitation wavelengths of 475 nm (d) and 620 nm (e).

3.2. Multi-Functional Properties of uPA/Pep/TA NPs. The assembled uPA/Pep/TA NPs contain a PAS-based peptide, which is low-fouling[40] and contains two thrombin-cleavable sequences (ELTPRGWRLE).[41] The biofunctionality of the uPA/Pep/TA NPs was systematically studied by examining the attenuated nonspecific activity of uPA and thrombin-responsive release of uPA, as well as the cellular behavior in vitro and biodistribution and blood clearance in vivo of the NPs.

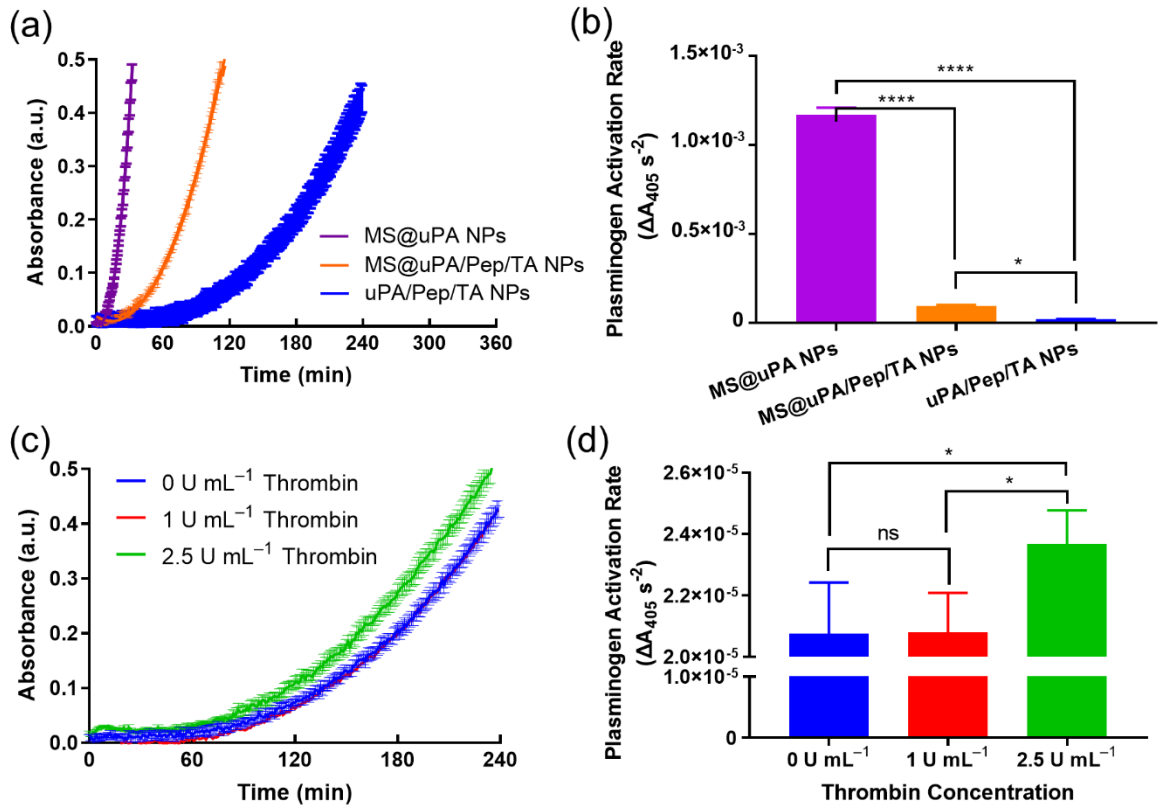

Figure 5. (a) Plasminogen activation assay absorbance curves at 405 nm for MS@uPA NPs, MS@uPA/Pep/TA NPs, and uPA/Pep/TA NPs and (b) the corresponding fitted plasminogen activation rates. (c) Plasminogen activation assay absorbance curves at 405 nm and (d) the corresponding fitted plasminogen activation rates of uPA/Pep/TA NPs at different thrombin

concentrations in the assay test. In (a, c), data are presented as mean ± standard error of the mean (n = 3 for each measured timepoint). In (a), data are fitted to a second-order polynomial (quadratic) nonlinear regression ($Y = A + BX + CX^2$) (black curve). In (b, d), data are presented as mean ± SD (n = 3) and analyzed by one-way ANOVA with uncorrected Fisher's least significance difference post-hoc test, where $p > 0.05$ (ns), $p < 0.05$ (*), $p < 0.01$ (**), $p < 0.001$ (***), and $p < 0.0001$ (****).

3.2.1. Attenuated Nonspecific uPA Activity and Thrombin-Responsive Performance. As a proof-of-concept that the NPs can function as a thrombolytic drug delivery platform, we assessed the capacity of the uPA-loaded NPs to generate the clot-busting enzyme, plasmin. Additionally, we aimed to demonstrate a thrombin-dependent mode of plasminogen activation via the thrombin-cleavable peptides embedded in the NPs. Figure 5a,b shows the plasmin generation activity of uPA-loaded NPs (which can be compared to plasmin generation by free uPA, displayed in Figure S4 as a reference). When mixed with plasminogen and the plasmin-specific chromogenic substrate S-2251,[42] all uPA-loaded NPs (MS@uPA NPs, MS@uPA/Pep/TA NPs, and uPA/Pep/TA NPs) demonstrated reduced rates of plasminogen activation compared with the free uPA control (12.9×10^{-3} ΔA_{405} s^{-2}). Specifically, among the three NPs examined, MS@uPA NPs (without TA) displayed the highest rate of plasminogen activation (1.17×10^{-3} ΔA_{405} s^{-2}), and MS@uPA/Pep/TA NPs and uPA/Pep/TA NPs both displayed significantly lower rates (9.63×10^{-5} ΔA_{405} s^{-2} and 2.07×10^{-5} ΔA_{405} s^{-2}, respectively; $p < 0.0001$). The high plasminogen activation rates displayed by MS@uPA NPs is expected because of the absence of a protective polyphenol-based coating, allowing greater accessibility of the loaded uPA enzyme to the surrounding plasminogen substrate. This result also confirms that uPA maintains its enzymatic function to drive thrombolysis following loading in the MS NP templates.

The lower plasminogen activation rate observed for MS@uPA/Pep/TA NPs relative to that for MS@uPA NPs (i.e., after vs. before the polyphenol-based process) represents a reduction of more than 90%. However, a loss of only 37% uPA was measured during the polyphenol-based process (Table S1). These findings suggest that the presence of the polyphenol limits the accessibility of uPA to the external environment because of the hydrophobic interactions among uPA, peptide, and TA. The incubation of the NPs in 2 M HF/3 M NH_4F buffer solution during template removal resulted in no apparent difference in plasminogen activity between the HF-treated and DPBS-treated (control) uPA-loaded carboxylic acid-functionalized polystyrene particles (7.67×10^{-4} $\Delta A_{405}\ s^{-2}$ and 8.21×10^{-4} $\Delta A_{405}\ s^{-2}$, respectively, with a particle concentration of 1.7×10^6 particles mL^{-1}), as shown in Figure S5. This finding suggests that the protein function is preserved after HF treatment (2 M HF/3 M NH4F buffer solution), which is consistent with our previous studies on the MS-templated assembly of protein NPs.[9] Therefore, the lower plasminogen activity of uPA/Pep/TA NPs (2.07×10^{-5} $\Delta A_{405}\ s^{-2}$) relative to that of the MS@uPA/Pep/TA NPs (9.63×10^{-5} $\Delta A_{405}\ s^{-2}$) is attributed to a loss of uPA with the additional washing steps required with removal of the MS NP templates.

During blood clotting, platelet activation is reported to occur in vivo at thrombin concentrations of ~ 0.1 U mL^{-1} and up to over 10 U mL^{-1}.[43] To further assess the thrombin-responsiveness of the uPA/Pep/TA NPs, thrombin at different concentrations (0, 1, 2.5 U mL^{-1}) was added to the plasminogen activation assay. The thrombin-responsiveness of the NPs was designed by incorporating a peptide with two thrombin-cleavable sequences (ELTPRGWRLE) during the polyphenol-based process. Theoretically, the TA-crosslinked thrombin-responsive peptide could serve as a physical barrier between uPA and plasminogen in bulk. Thus, the polyphenol-based peptide is expected to inhibit the plasminogen activation of uPA until thrombin-mediated

degradation of the peptide occurs, leading to an accelerated plasminogen activation rate of uPA. From the results in Figure 5c,d, we observed a higher plasminogen activation rate when the uPA/Pep/TA NPs were treated with 2.5 U mL^{-1} thrombin (2.37×10^{-5} ΔA_{405} s^{-2}) than with 1 or 0 U mL^{-1} thrombin (2.07×10^{-5} ΔA_{405} s^{-2} and 2.08×10^{-5} ΔA_{405} s^{-2}, respectively; $p < 0.05$). Notably, this thrombin-responsive increase was absent over the same concentration range in the template-containing NPs (MS@uPA/Pep/TA NPs) (data not shown). A possible explanation for this phenomenon may relate to the influence of the MS NP template, whereby thrombin may adsorb onto accessible surface of the MS NPs, which is consistent with observations from our previous study on protein adsorption on polymer-coated MS NPs.[34,35]

Removal of the MS NP template provided the ability of the uPA/Pep/TA NPs to deliver uPA cargo in a thrombin-responsive manner. However, given that plasminogen activation was detected in the absence of thrombin, additional work is warranted to further reduce nonspecific uPA activity. This is particularly important for the delivery of thrombolytic agents to minimize premature release of the drug and prevent nonspecific plasminogen activation, which can cause adverse events such as haemorrhagic complications.[15] Additionally, further optimization studies are required to generate highly sensitive thrombin responses at lower thrombin concentrations (e.g., 0.1–1 U mL^{-1}), representing the physiological thrombus microenvironment.[44,45]

3.2.2. In Vitro Cellular Cytotoxicity and Association. The cellular cytotoxicity of the different particle systems, their nonspecific cellular association, and in vivo biodistribution were investigated using BSA as cargo. The drug formulations that are employed in clinical-grade biological therapies often contain high amounts of albumin,[46,47] including clinically used uPA (U-FRAG), according to the sodium dodecyl sulphate–polyacrylamide gel electrophoresis results (Figure S6), and its product specifications.[48] As reported in the literature, the presence of excess

albumin excipient in the formulation of uPA preserves the enzymatic activity of uPA as opposed to uPA formulations without albumin.[49] Therefore, in our biological investigations, we used albumin-loaded NPs. This allows the study of nanocarriers with a more similar composition to those encapsulating clinical uPA (as described previously), while also expanding the scope of our investigation to demonstrate the encapsulation capacity of our NPs for potentially other biological therapy drugs that are formulated with excess albumin.

The morphologies of the fluorescently labeled protein-loaded NPs MS@BSA NPs, MS@BSA/Pep/TA NPs, and BSA/Pep/TA NPs, as characterized by TEM and DLS, are shown in Figure S7a–c. The sizes of these particles were similar to those of the uPA-loaded NPs (i.e., MS@uPA NPs, MS@uPA/Pep/TA NPs, and uPA/Pep/TA NPs). The stability of the BSA/Pep/TA NPs was examined by monitoring any changes in particle size using DLS. Figure S7d shows that there is no difference in size of the BSA/Pep/TA NPs after incubation in human plasma for 0 and 24 h at 37 °C, suggesting that the NPs are stable in human plasma. The cellular cytotoxicity and association of the fluorescently labeled BSA-loaded NPs were examined by incubating the particles with two cell lines, i.e., Raw 264.7 cells and THP-1 cells, which are commonly used in phagocytosis and immune modulation studies. RAW 264.7 is a mouse-derived macrophage cell line and THP-1 is a human monocytic cell line. As observed from Figure 6a and b, all three particle systems displayed negligible cytotoxicity even after incubation at a high cell-to-NP ratio (1:1000). This can be ascribed to the highly biocompatible nature of all the components of the NPs (i.e., MS, TA, peptide, and protein). To better understand the bio–nano interactions of the NPs, their cell association was evaluated by flow cytometry (Figure 6c). In the first hour of incubation, all three particle systems displayed similar, low cell association (<5%) with both cell lines owing to the small size and low density of the particle systems. In contrast, significant differences were

observed after incubation for 12 h. Among the three particle systems, the BSA/Pep/TA NPs displayed the lowest association with both cell lines, 43% for Raw 264.7 cells and 7% for THP-1 cells. Both MS@BSA NPs and MS@BSA/Pep/TA NPs displayed high association (over 80%) with Raw 264.7 cells but considerably lower cell association with THP-1 cells (i.e., ~25% and <10%, respectively).

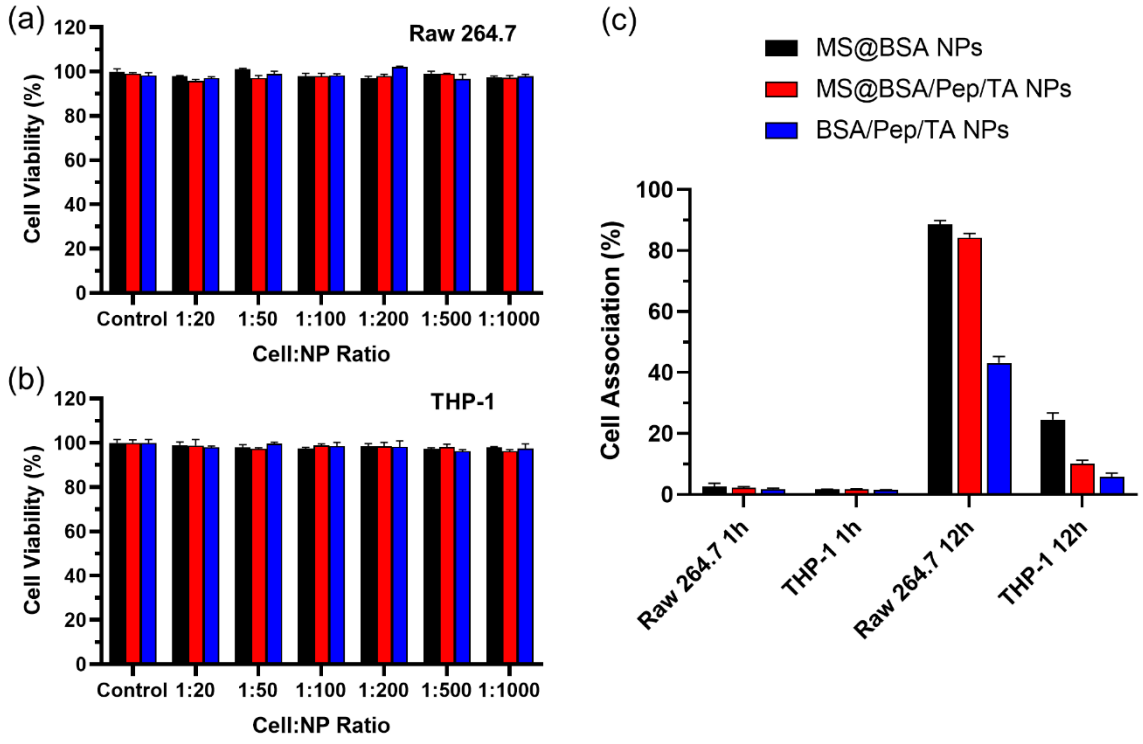

Figure 6. (a, b) Cytotoxicity and (c) cell association (% cells) of the particle systems MS@BSA NPs, MS@BSA/Pep/TA NPs, and BSA/Pep/TA NPs evaluated by two cell lines Raw 264.7 cells and THP-1 cells. In (c), cell association was measured by flow cytometry after incubation of the particles systems for 1 or 12 h at 37 °C in medium.

3.2.3. In Vivo Biodistribution and Blood Clearance. To determine the behavior of the NPs in vivo, biodistribution and blood clearance studies were performed. The biodistribution results in Figure 7a and c show that the % injected dose per gram for both MS@BSA/Pep/TA NPs and BSA/Pep/TA NPs was highest in the liver at 24 h post injection, followed by the spleen ($p < 0.001$

with or without the MS NP template, respectively), and the remaining organs. No significant differences were observed between the lung, kidney, and heart across all timepoints for both NP types. Furthermore, the hepatic accumulation of both NP types increased over time, with significantly higher uptake after 24 h relative to 1 h (2.2- and 1.7-fold increase for MS@BSA/Pep/TA NPs and BSA/Pep/TA NPs, respectively; $p < 0.0001$). These findings indicate a predominantly hepatic processing and clearance mechanism for our NPs, consistent with other NP studies.[50–55] Notably, the template-containing NPs (MS@BSA/Pep/TA NPs) displayed significantly higher accumulation than their template-free counterpart (BSA/Pep/TA NPs) at the 24 h timepoint in the liver (487.5 ± 84.5 versus 148.1 ± 0.6 % injected dose g^{-1}, respectively, $p < 0.0001$) and spleen (289.6 ± 82.4 versus 97.6 ± % injected dose g^{-1}, respectively, $p = 0.0004$). This is consistent with our previous observations on poly(ethylene glycol) (PEG)-based NPs.[56] Template-free PEG NPs showed extended in vivo circulation times and lower accumulation in the liver and the spleen than their template-containing counterpart (PEGylated MS NPs). The presence of the MS NP template influences the surface properties and stiffness of the NPs, likely leading to the formation of a specific (and different) protein corona in blood and inducing immune cell association, as previously observed with other MS-templated polymer NPs.[34,35] Our in vitro studies in Figure 6c further support that the MS@BSA/Pep/TA NPs may deposit more readily within blood-clearing organs owing to their higher cell association (approximately 2-fold at 12 h) when compared with the BSA/Pep/TA NPs. However, a detailed study on the composition and impact of a protein corona on the pharmacokinetic profiles of the BSA/Pep/TA NPs is beyond the scope of the present work. In addition, we note that the higher hepatic accumulation of MS@BSA/Pep/TA NPs than that of BSA/Pep/TA NPs could also, in part, derive from the higher concentration of MS@BSA/Pep/TA NPs injected (~4.7-fold higher than BSA/Pep/TA NPs; this is

a result of material loss during the MS NP template removal procedure). Thus, further validation of these findings is required with identical NP amounts in future studies.

Blood clearance analysis provided further insights into the in vivo performance of our NPs. There were distinct differences in the observed blood clearance curves, with the MS@BSA/Pep/TA NPs and BSA/Pep/TA NPs presenting as a one-phase (R^2 = 0.9981) and two-phase (R^2 = 0.9975) exponential decay, respectively. The calculated circulating half-life was 46 s and 1 min for MS@BSA/Pep/TA NPs and BSA/Pep/TA NPs, respectively. The temporal investigation of the NP blood clearance profiles in Figure 7b revealed that the template-containing MS@BSA/Pep/TA NPs were more rapidly cleared than the template-free BSA/Pep/TA NPs—90% clearance achieved within 5 min for MS@BSA/Pep/TA NPs compared with 60 min for BSA/Pep/TA NPs for the same clearance level. However, it should be noted that both NP types showed a rapid clearance profile, with ~80% and ~70% of the MS@BSA/Pep/TA NPs and BSA/Pep/TA NPs cleared, respectively, within the first 2.5 min post injection (20.6 ± 7.5 and 30.6 ± 3.6 % injected dose, respectively, p = 0.0075). Collectively, the results suggest that a rapid, template-independent liver clearance mechanism operates with these multi-biofunctional polyphenol-based NPs.

Considering the fouling properties of MS@BSA/Pep/TA NPs and BSA/Pep/TA NPs and the biodistribution and blood clearance results, we conclude that the template-free NP system presents with more favorable resistance to nonspecific cell association (at the 12 h timepoint) than the template-containing NP system. BSA/Pep/TA NPs featured lower organ accumulation profiles and a delayed blood clearance when compared with MS@BSA/Pep/TA NPs. Nevertheless, additional dose optimization studies are needed to fully confirm this observation.

Nanoparticle technologies continue to demonstrate immense promise in delivering thrombolytic therapy to treat thrombotic disease, which includes offering improved efficacy and reduction in serious complications.[23] Furthermore, the encapsulation of thrombolytic agents in NPs offers the potential to design prophylactic therapeutic approaches for administering thrombolytic therapy, which is not currently available due to the inherent risks involved with free thrombolytic agents in circulation. The successful implementation of a prophylactic therapeutic approach for thrombolytic therapy offers future thrombosis patients with an increased chance of survival and improved quality of life post-diagnosis.

Future directions aim to build upon these findings to further optimize the drug release kinetics (extended to include physiologically relevant environments such as plasma and/or serum) and eventually apply our NPs to in vivo models of thrombosis and thrombotic disease.

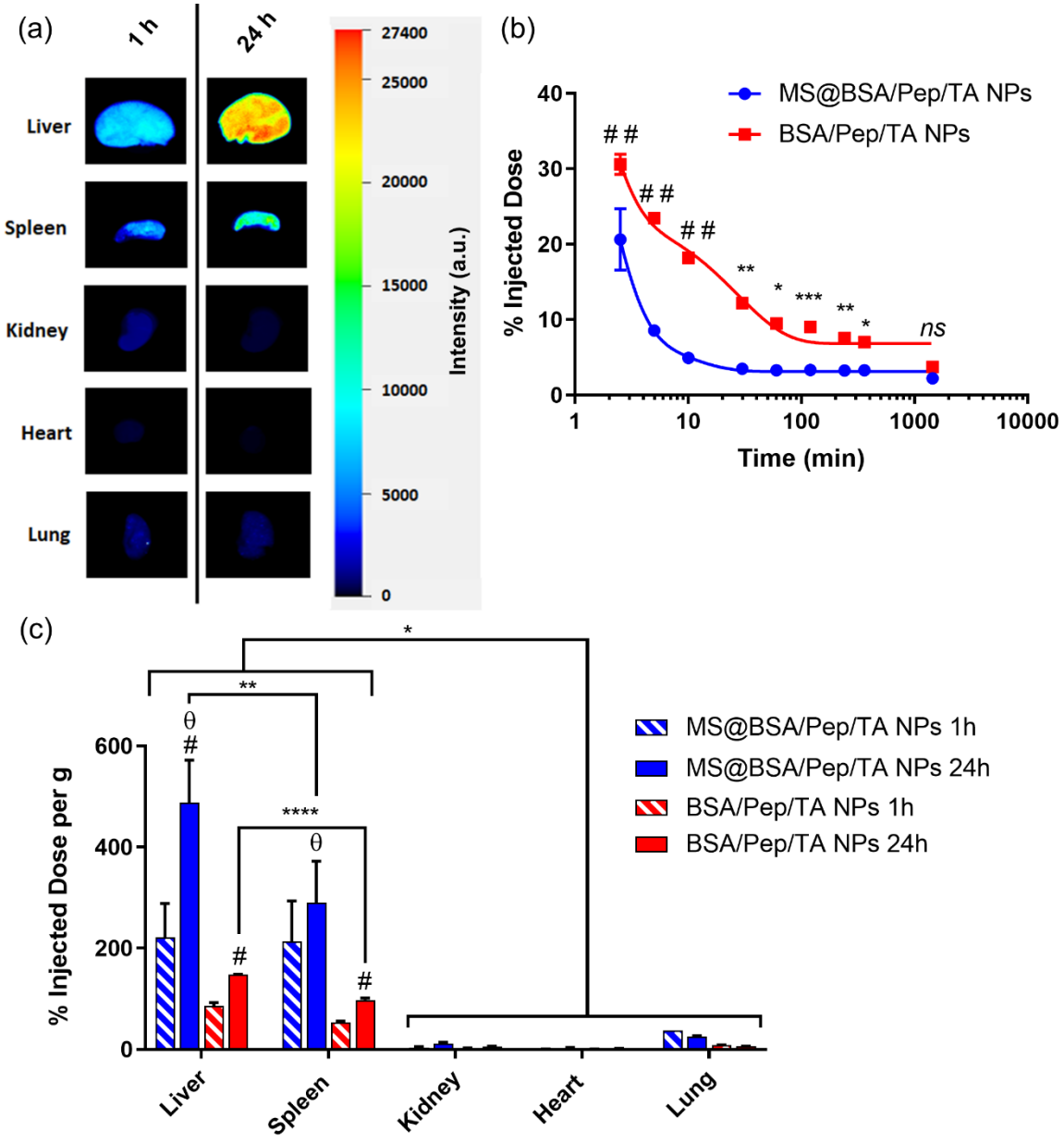

Figure 7. (a) Representative fluorescence scans of the liver, spleen, kidney, heart, and lung at 1 and 24 h post injection with MS@BSA/Pep/TA NPs. (b) Blood clearance and (c) biodistribution profiles of MS@BSA/Pep/TA NPs and BSA/Pep/TA NPs. In (b, c), data are shown as the mean ± SD for MS@BSA/Pep/TA NPs 1h (n = 2), MS@BSA/Pep/TA NPs 24h (n = 4), BSA/Pep/TA NPs 1h (n = 3), and BSA/Pep/TA NPs 24h (n = 2). In (b) $^{\#\#}p < 0.01$ compared with the other NP type at the corresponding timepoint by two-way ANOVA with Tukey's post-hoc test; $^{*}p < 0.05$, $^{**}p$

< 0.01, ***$p < 0.001$, and ns by unpaired Student's *t*-test. In (c), unless specified, *$p < 0.05$, ** $p < 0.01$, and ****$p < 0.0001$ compared with all other organs and timepoints with the same NP type; $^{\#}p < 0.001$ comparing organ-specific 1 h and 24 h timepoints for each NP type; and $^{\theta}p < 0.001$ comparing different NPs at identical timepoints in the same organ; all by two-way ANOVA with Tukey's post-hoc test.

4. CONCLUSION

Bioresponsive uPA/Pep/TA NPs were synthesized using a polyphenol-based method. The NPs were monodisperse in size with a diameter of ~250 nm. The plasminogen activity of the thrombolytic protein drug uPA loaded in the NPs was significantly attenuated and generated a positive response to the surrounding thrombin concentration owing to the two thrombin-cleavable sequences of the polyphenol-crosslinked peptide. The behavior of the NPs in biological environments was assessed through in vitro cellular cytotoxicity and association studies using Raw 264.7 and THP-1 cell lines and in vivo biodistribution and blood clearance studies using BSA as the model drug. The bioresponsive polyphenol-based NPs displayed reduced nonspecific cell association and a delayed blood clearance, making them potentially suitable for the desired thrombolysis applications.

ASSOCIATED CONTENT

Supporting Information. SEM and TEM images, nitrogen adsorption–desorption isotherms, and pore size distributions of MS NP templates; standard curves of AF647-uPA; plasminogen activation assay measurement of free uPA and uPA-loaded polystyrene particles; dodecyl sulphate–polyacrylamide gel electrophoresis results of U-FRAG; TEM and DLS data of BSA-loaded NPs; fluorescence intensity and calculated concentrations of uPA and peptide in the NPs; and MIRIBEL checklist for reporting research in bio–nano science.

AUTHOR INFORMATION

Corresponding Author

*fcaruso@unimelb.edu.au (F. C.); christoph.hagemeyer@monash.edu (C. E. H.)

Author Contributions

The manuscript was written through contributions of all authors. All authors have given approval to the final version of the manuscript. ‡H.Y., J.S.P., and J.Z. contributed equally to this work.

Notes

The authors have no conflicts of interest to declare.

ACKNOWLEDGMENT

We thank Dr. Karen Alt, Ms. Anukreity Ale, Dr. Christina Cortez-Jugo, Dr. Yiyuan Han, and Ms. Jingqu Chen for helpful discussions and/or support with the characterization studies. This research was funded and supported by a National Health and Medical Research Council (NHMRC) Project Grant (GNT1138361, C.E.H. and F.C.). F.C. and C.E.H. acknowledge the awards of an NHMRC Senior Principal Research Fellowship (GNT1135806) and an NHMRC Research Fellowship (GNT1154270), respectively. J.S.P acknowledges support from Australian Rotary Health, Rotary District 9830 and the Australian Government Research Training Program (RTP) Scholarship.

REFERENCES

(1) Benjamin, E. J.; Virani, S. S.; Callaway, C. W.; Chamberlain, A. M.; Chang, A. R.; Cheng, S.; Chiuve, S. E.; Cushman, M.; Delling, F. N.; Deo, R.; de Ferranti, S. D.; Ferguson, J. F.; Fornage, M.; Gillespie, C.; Isasi, C. R.; Jiménez, M. C.; Jordan, L. C.;

Judd, S. E.; Lackland, D.; Lichtman, J. H.; Lisabeth, L.; Liu, S.; Longenecker, C. T.; Lutsey, P. L.; Mackey, J. S.; Matchar, D. B.; Matsushita, K.; Mussolino, M. E.; Nasir, K.; O'Flaherty, M.; Palaniappan, L. P.; Pandey, A.; Pandey, D. K.; Reeves, M. J.; Ritchey, M. D.; Rodriguez, C. J.; Roth, G. A.; Rosamond, W. D.; Sampson, U. K. A.; Satou, G. M.; Shah, S. H.; Spartano, N. L.; Tirschwell, D. L.; Tsao, C. W.; Voeks, J. H.; Willey, J. Z.; Wilkins, J. T.; Wu, J. H. Y.; Alger, H. M.; Wong, S. S.; Muntner, P. Heart Disease and Stroke Statistics—2018 Update: A Report From the American Heart Association. *Circulation* **2018**, *137*, E67–E492.

(2) Ma, H.; Jiang, Z.; Xu, J.; Liu, J.; Guo, Z.-N. Targeted Nano-Delivery Strategies for Facilitating Thrombolysis Treatment in Ischemic Stroke. *Drug Delivery* **2021**, *28*, 357–371.

(3) Kim, M. K.; Han, K.; Kim, H.-S.; Park, Y.-M.; Kwon, H.-S.; Yoon, K.-H.; Lee, S.-H. Cholesterol Variability and the Risk of Mortality, Myocardial Infarction, and Stroke: A Nationwide Population-Based Study. *Eur. Heart J.* **2017**, *38*, 3560–3566.

(4) Mackman, N. Triggers, Targets and Treatments for Thrombosis. *Nature* **2008**, *451*, 914–918.

(5) Stewart, M. P.; Sharei, A.; Ding, X.; Sahay, G.; Langer, R.; Jensen, K. F. In Vitro and Ex Vivo Strategies for Intracellular Delivery. *Nature* **2016**, *538*, 183–192.

(6) Hagemeyer, C. E.; Lisman, T.; Kwaan, H. C. Nanomedicine in Thrombosis and Hemostasis: The Future of Nanotechnology in Thrombosis and Hemostasis Research and Clinical Applications. *Semin. Thromb. Hemostasis* **2020**, *46*, 521–523.

(7) Shin, M.; Lee, H.-A.; Lee, M.; Shin, Y.; Song, J.-J.; Kang, S.-W.; Nam, D.-H.; Jeon, E. J.; Cho, M.; Do, M.; Park, S.; Lee, M. S.; Jang, J.-H.; Cho, S.-W.; Kim, K.-S.; Lee, H.

Targeting Protein and Peptide Therapeutics to the Heart via Tannic Acid Modification. *Nat. Biomed. Eng.* **2018**, *2*, 304–317.

(8) Bai, Y.; Luo, Q.; Liu, J. Protein Self-Assembly via Supramolecular Strategies. *Chem. Soc. Rev.* **2016**, *45*, 2756–2767.

(9) Han, Y.; Zhou, J.; Hu, Y.; Lin, Z.; Ma, Y.; Richardson, J. J.; Caruso, F. Polyphenol-Based Nanoparticles for Intracellular Protein Delivery via Competing Supramolecular Interactions. *ACS Nano* **2020**, *14*, 12972–12981.

(10) Ali, M. R.; Salim Hossain, M.; Islam, M. A.; Saiful Islam Arman, M.; Sarwar Raju, G.; Dasgupta, P.; Noshin, T. F. Aspect of Thrombolytic Therapy: A Review. *Sci. World J.* **2014**, *2014*, 1–8.

(11) Powers, W. J.; Rabinstein, A. A.; Ackerson, T.; Adeoye, O. M.; Bambakidis, N. C.; Becker, K.; Biller, J.; Brown, M.; Demaerschalk, B. M.; Hoh, B.; Jauch, E. C.; Kidwell, C. S.; Leslie-Mazwi, T. M.; Ovbiagele, B.; Scott, P. A.; Sheth, K. N.; Southerland, A. M.; Summers, D. V.; Tirschwell, D. L. 2018 Guidelines for the Early Management of Patients with Acute Ischemic Stroke: A Guideline for Healthcare Professionals from the American Heart Association/American Stroke Association. *Stroke* **2018**, *49*, e46–e110.

(12) Kadir, R. R. A.; Bayraktutan, U. Urokinase Plasminogen Activator: A Potential Thrombolytic Agent for Ischaemic Stroke. *Cell. Mol. Neurobiol.* **2020**, *40*, 347–355.

(13) Colucci, M.; Paramo, J. A.; Collen, D. Inhibition of One-Chain and Two-Chain Forms of Human Tissue-Type Plasminogen Activator by the Fast-Acting Inhibitor of Plasminogen Activator In Vitro and In Vivo. *J. Lab. Clin. Med.* **1986**, *108*, 44–52.

(14) Chapin, J. C.; Hajjar, K. A. Fibrinolysis and the Control of Blood Coagulation. *Blood Rev.* **2015**, *29*, 17–24.

(15) Ebben, H. P.; van Burink, M. V.; Jongkind, V.; Mouwen, D. E.; Udding, J.; Wisselink, W.; Kievit, J. K.; Wiersema, A. M.; Yeung, K. Efficacy versus Complications in Arterial Thrombolysis. *Ann. Vasc. Surg.* **2018**, *48*, 111–118.

(16) Dong, Q.; Dong, Y.; Liu, L.; Xu, A.; Zhang, Y.; Zheng, H.; Wang, Y. The Chinese Stroke Association Scientific Statement: Intravenous Thrombolysis in Acute Ischaemic Stroke. *Stroke Vasc. Neurol.* **2017**, *2*, 147–159.

(17) Korin, N.; Gounis, M. J.; Wakhloo, A. K.; Ingber, D. E. Targeted Drug Delivery to Flow-Obstructed Blood Vessels Using Mechanically Activated Nanotherapeutics. *JAMA Neurol.* **2015**, *72*, 119–122.

(18) Epshtein, M.; Korin, N. Shear Targeted Drug Delivery to Stenotic Blood Vessels. *J. Biomech.* **2017**, *50*, 217–221.

(19) Absar, S.; Kwon, Y. M.; Ahsan, F. Bio-Responsive Delivery of Tissue Plasminogen Activator for Localized Thrombolysis. *J. Controlled Release* **2014**, *177*, 42–50.

(20) Gunawan, S. T.; Kempe, K.; Bonnard, T.; Cui, J.; Alt, K.; Law, L. S.; Wang, X.; Westein, E.; Such, G. K.; Peter, K.; Hagemeyer, C. E.; Caruso, F. Multifunctional Thrombin-Activatable Polymer Capsules for Specific Targeting to Activated Platelets. *Adv. Mater.* **2015**, *27*, 5153–5157.

(21) Wang, X.; Palasubramaniam, J.; Gkanatsas, Y.; Hohmann, J. D.; Westein, E.; Kanojia, R.; Alt, K.; Huang, D.; Jia, F.; Ahrens, I.; Medcalf, R. L.; Peter, K.; Hagemeyer, C. E. Towards Effective and Safe Thrombolysis and Thromboprophylaxis. *Circ. Res.* **2014**, *114*, 1083–1093.

(22) Huang, Y.; Yu, L.; Ren, J.; Gu, B.; Longstaff, C.; Hughes, A. D.; Thom, S. A.; Xu, X. Y.; Chen, R. An Activated-Platelet-Sensitive Nanocarrier Enables Targeted Delivery of

Tissue Plasminogen Activator for Effective Thrombolytic Therapy. *J. Controlled Release* **2019**, *300*, 1–12.

(23) Palazzolo, J. S.; Westein, E.; Hagemeyer, C. E.; Wang, T.-Y. Targeting Nanotechnologies for the Treatment of Thrombosis and Cardiovascular Disease. *Semin. Thromb. Hemostasis* **2020**, *46*, 606–621.

(24) Cheng, R.; Huang, W.; Huang, L.; Yang, B.; Mao, L.; Jin, K.; ZhuGe, Q.; Zhao, Y. Acceleration of Tissue Plasminogen Activator-Mediated Thrombolysis by Magnetically Powered Nanomotors. *ACS Nano* **2014**, *8*, 7746–7754.

(25) Griffin, M. T.; Zhu, Y.; Liu, Z.; Aidun, C. K.; Ku, D. N. Inhibition of High Shear Arterial Thrombosis by Charged Nanoparticles. *Biomicrofluidics* **2018**, *12*, 042210.

(26) Molloy, C. P.; Yao, Y.; Kammoun, H.; Bonnard, T.; Hoefer, T.; Alt, K.; Tovar-Lopez, F.; Rosengarten, G.; Ramsland, P. A.; van der Meer, A. D.; van den Berg, A.; Murphy, A. J.; Hagemeyer, C. E.; Peter, K.; Westein, E. Shear-Sensitive Nanocapsule Drug Release for Site-Specific Inhibition of Occlusive Thrombus Formation. *J. Thromb. Haemostasis* **2017**, *15*, 972–982.

(27) Zhou, J.; Lin, Z.; Ju, Y.; Rahim, M. A.; Richardson, J. J.; Caruso, F. Polyphenol-Mediated Assembly for Particle Engineering. *Acc. Chem. Res.* **2020**, *53*, 1269–1278.

(28) Ejima, H.; Richardson, J. J.; Caruso, F. Metal-Phenolic Networks as a Versatile Platform to Engineer Nanomaterials and Biointerfaces. *Nano Today* **2017**, *12*, 136–148.

(29) Rahim, M. A.; Kristufek, S. L.; Pan, S.; Richardson, J. J.; Caruso, F. Phenolic Building Blocks for the Assembly of Functional Materials. *Angew. Chem., Int. Ed.* **2019**, *58*, 1904–1927.

(30) Guo, J.; Tardy, B. L.; Christofferson, A. J.; Dai, Y.; Richardson, J. J.; Zhu, W.; Hu, M.;

Ju, Y.; Cui, J.; Dagastine, R. R.; Yarovsky, I.; Caruso, F. Modular Assembly of Superstructures from Polyphenol-Functionalized Building Blocks. *Nat. Nanotechnol.* **2016**, *11*, 1105–1111.

(31) Wu, D.; Zhou, J.; Creyer, M. N.; Yim, W.; Chen, Z.; Messersmith, P. B.; Jokerst, J. V. Phenolic-Enabled Nanotechnology: Versatile Particle Engineering for Biomedicine. *Chem. Soc. Rev.* **2021**, *50*, 4432–4483.

(32) Ju, Y.; Cui, J.; Sun, H.; Müllner, M.; Dai, Y.; Guo, J.; Bertleff-Zieschang, N.; Suma, T.; Richardson, J. J.; Caruso, F. Engineered Metal-Phenolic Capsules Show Tunable Targeted Delivery to Cancer Cells. *Biomacromolecules* **2016**, *17*, 2268–2276.

(33) Ju, Y.; Cortez-Jugo, C.; Chen, J.; Wang, T. Y.; Mitchell, A. J.; Tsantikos, E.; Bertleff-Zieschang, N.; Lin, Y. W.; Song, J.; Cheng, Y.; Mettu, S.; Rahim, M. A.; Pan, S.; Yun, G.; Hibbs, M. L.; Yeo, L. Y.; Hagemeyer, C. E.; Caruso, F. Engineering of Nebulized Metal–Phenolic Capsules for Controlled Pulmonary Deposition. *Adv. Sci.* **2020**, *7*, 1902650.

(34) Song, J.; Ju, Y.; Amarasena, T. H.; Lin, Z.; Mettu, S.; Zhou, J.; Rahim, M. A.; Ang, C. S.; Cortez-Jugo, C.; Kent, S. J.; Caruso, F. Influence of Poly(ethylene Glycol) Molecular Architecture on Particle Assembly and Ex Vivo Particle–Immune Cell Interactions in Human Blood. *ACS Nano* **2021**, *15*, 10025–10038.

(35) Ju, Y.; Kelly, H. G.; Dagley, L. F.; Reynaldi, A.; Schlub, T. E.; Spall, S. K.; Bell, C. A.; Cui, J.; Mitchell, A. J.; Lin, Z.; Wheatley, A. K.; Thurecht, K. J.; Davenport, M. P.; Webb, A. I.; Caruso, F.; Kent, S. J. Person-Specific Biomolecular Coronas Modulate Nanoparticle Interactions with Immune Cells in Human Blood. *ACS Nano* **2020**, *14*, 15723–15737.

(36) Yang, Y.; Bernardi, S.; Song, H.; Zhang, J.; Yu, M.; Reid, J. C.; Strounina, E.; Searles, D. J.; Yu, C. Anion Assisted Synthesis of Large Pore Hollow Dendritic Mesoporous Organosilica Nanoparticles: Understanding the Composition Gradient. *Chem. Mater.* **2016**, *28*, 704–707.

(37) Chen, J.; Li, J.; Zhou, J.; Lin, Z.; Cavalieri, F.; Czuba-Wojnilowicz, E.; Hu, Y.; Glab, A.; Ju, Y.; Richardson, J. J.; Caruso, F. Metal–Phenolic Coatings as a Platform to Trigger Endosomal Escape of Nanoparticles. *ACS Nano* **2019**, *13*, 11653–11664.

(38) Evans, G. O. Removal of Blood from Laboratory Mammals and Birds. *Lab. Anim.* **1994**, *28*, 178–179.

(39) Faria, M.; Björnmalm, M.; Thurecht, K. J.; Kent, S. J.; Parton, R. G.; Kavallaris, M.; Johnston, A. P. R.; Gooding, J. J.; Corrie, S. R.; Boyd, B. J.; Thordarson, P.; Whittaker, A. K.; Stevens, M. M.; Prestidge, C. A.; Porter, C. J. H.; Parak, W. J.; Davis, T. P.; Crampin, E. J.; Caruso, F. Minimum Information Reporting in Bio–Nano Experimental Literature. *Nat. Nanotechnol.* **2018**, *13*, 777–785.

(40) Schlapschy, M.; Binder, U.; Borger, C.; Theobald, I.; Wachinger, K.; Kisling, S.; Haller, D.; Skerra, A. PASylation: A Biological Alternative to PEGylation for Extending the Plasma Half-Life of Pharmaceutically Active Proteins. *Protein Eng., Des. Sel.* **2013**, *26*, 489–501.

(41) Gallwitz, M.; Enoksson, M.; Thorpe, M.; Hellman, L. The Extended Cleavage Specificity of Human Thrombin. *PLoS One* **2012**, *7*, e31756.

(42) Friberger, P.; Knös, M.; Gustavsson, S.; Aurell, L.; Claeson, G. Methods for Determination of Plasmin, Antiplasmin and Plasminogen by Means of Substrate S-2251. *Pathophysiol. Haemostasis Thromb.* **1978**, *7*, 138–145.

(43) Mann, K. G.; Brummel, K.; Butenas, S. What Is All That Thrombin For? *J. Thromb. Haemostasis* **2003**, *1*, 1504–1514.

(44) Mutch, N. J.; Robbie, L. A.; Booth, N. A. Human Thrombi Contain an Abundance of Active Thrombin. *Thromb. Haemostasis* **2001**, *86*, 1028–1034.

(45) Wolberg, A. S.; Campbell, R. A. Thrombin Generation, Fibrin Clot Formation and Hemostasis. *Transfus. Apher. Sci.* **2008**, *38*, 15–23.

(46) Tarelli, E.; Mire-Sluis, A.; Tivnann, H. A.; Bolgiano, B.; Crane, D. T.; Gee, C.; Lemercinier, X.; Athayde, M. L.; Sutcliffe, N.; Corran, P. H.; Rafferty, B. Recombinant Human Albumin as a Stabilizer for Biological Materials and for the Preparation of International Reference Reagents. *Biologicals* **1998**, *26*, 331–346.

(47) Sleep, D. Albumin and Its Application in Drug Delivery. *Expert Opin. Drug Delivery* **2015**, *12*, 793–812.

(48) Bharat Serums and Vaccines Limited. *Urokinase For Injection (U-FRAG, LYOPHILIZED)*. https://www.bharatserums.com/assets/pdf/products/U-FRAG(Lyo).pdf (accessed July 2019).

(49) Patel, J. P. Urokinase: Stability Studies in Solution and Lyophilized Formulations. *Drug Dev. Ind. Pharm.* **1990**, *16*, 2613–2626.

(50) Nold, P.; Hartmann, R.; Feliu, N.; Kantner, K.; Gamal, M.; Pelaz, B.; Hühn, J.; Sun, X.; Jungebluth, P.; del Pino, P.; Hackstein, H.; Macchiarini, P.; Parak, W. J.; Brendel, C. Optimizing Conditions for Labeling of Mesenchymal Stromal Cells (MSCs) with Gold Nanoparticles: A Prerequisite for In Vivo Tracking of MSCs. *J. Nanobiotechnol.* **2017**, *15*, 24.

(51) Wang, J.; Mao, W.; Lock, L. L.; Tang, J.; Sui, M.; Sun, W.; Cui, H.; Xu, D.; Shen, Y. The

Role of Micelle Size in Tumor Accumulation, Penetration, and Treatment. *ACS Nano* **2015**, *9*, 7195–7206.

(52) Brinkhuis, R. P.; Stojanov, K.; Laverman, P.; Eilander, J.; Zuhorn, I. S.; Rutjes, F. P. J. T.; van Hest, J. C. M. Size Dependent Biodistribution and SPECT Imaging of ^{111}In-Labeled Polymersomes. *Bioconjug. Chem.* **2012**, *23*, 958–965.

(53) He, Q.; Zhang, Z.; Gao, F.; Li, Y.; Shi, J. In Vivo Biodistribution and Urinary Excretion of Mesoporous Silica Nanoparticles: Effects of Particle Size and PEGylation. *Small* **2011**, *7*, 271–280.

(54) Cui, J.; Alt, K.; Ju, Y.; Gunawan, S. T.; Braunger, J. A.; Wang, T.-Y.; Dai, Y.; Dai, Q.; Richardson, J. J.; Guo, J.; Björnmalm, M.; Hagemeyer, C. E.; Caruso, F. Ligand-Functionalized Poly(ethylene Glycol) Particles for Tumor Targeting and Intracellular Uptake. *Biomacromolecules* **2019**, *20*, 3592–3600.

(55) Cui, J.; Ju, Y.; Houston, Z. H.; Glass, J. J.; Fletcher, N. L.; Alcantara, S.; Dai, Q.; Howard, C. B.; Mahler, S. M.; Wheatley, A. K.; De Rose, R.; Brannon, P. T.; Paterson, B. M.; Donnelly, P. S.; Thurecht, K. J.; Caruso, F.; Kent, S. J. Modulating Targeting of Poly(ethylene Glycol) Particles to Tumor Cells Using Bispecific Antibodies. *Adv. Healthcare Mater.* **2019**, *8*, 1801607.

(56) Cui, J.; De Rose, R.; Alt, K.; Alcantara, S.; Paterson, B. M.; Liang, K.; Hu, M.; Richardson, J. J.; Yan, Y.; Jeffery, C. M.; Price, R. I.; Peter, K.; Hagemeyer, C. E.; Donnelly, P. S.; Kent, S. J.; Caruso, F. Engineering Poly(ethylene Glycol) Particles for Improved Biodistribution. *ACS Nano* **2015**, *9*, 1571–1580.

For Table of Contents Graphic Only